

A deterministic source of indistinguishable photons in a cluster state

Dan Cogan,¹ Zu-En Su,¹ Oded Kenneth,¹ and David Gershoni^{1,*}

¹*The Physics Department and the Solid State Institute,
Technion–Israel Institute of Technology, 3200003 Haifa, Israel*

Measurement-based quantum communication relies on the availability of highly entangled multi-photon cluster states. The inbuilt redundancy in the cluster allows communication between remote nodes using repeated local measurements, compensating for photon losses and probabilistic Bell-measurements. For feasible applications, the cluster generation should be fast, deterministic, and its photons - indistinguishable. We present a novel source based on a semiconductor quantum-dot device. The dot confines a heavy-hole, precessing in a finely tuned external weak magnetic field while periodically excited by a sequence of optical pulses. Consequently, the dot emits indistinguishable polarization-entangled photons, where the field strength optimizes the entanglement. We demonstrate Gigahertz rate deterministic generation of >90% indistinguishable photons in a cluster state with more than 10 photons characteristic entanglement-length.

A strong barrier to developing a full-fledged quantum network is the unavoidable photonic losses that exponentially limit the success probability of any quantum communication protocol with distance. Overcoming such exponential scaling is possible using the concept of quantum repeaters [1], in which entanglement swapping and purification performed at intermediate nodes enable entanglement distribution to distant nodes with photons [2, 3].

Inspired by measurement-based quantum computation [4], Zwerger and coworkers introduced the idea of measurement-based quantum repeaters [5]. This network architecture uses multi-photon entangled states, the cluster or graph states [6, 7], which can be distributed and mutually connected through Bell measurements. Recently, Azuma and coworkers [8] extended this idea by making the repeater graph exclusively photonic, thereby removing the need for a long-lived quantum memory. Graph states provide redundancy against photon loss and the probabilistic nature of photonic Bell measurements: If the first measurement fails, more trials will significantly increase the probability of success. An essential requirement from such graph-states is that the photons be indistinguishable. Developing devices capable of deterministically producing indistinguishable photonic graph states is, therefore, a scientific and technological challenge of the utmost importance [9–13].

Single and entangled photons can be generated via the spontaneous emission of an optical transition of an atom or an atom-like quantum emitter [14, 15] Artificial atoms such as semiconductor quantum dots (QDs) have demonstrated tremendous performance as they can be incorporated into electro-optical devices, which dovetail with the contemporary semiconductor-based industry. Semiconductor QD-based devices have shown unparalleled efficiency and rates (for a review see Ref. [16]), placing them as the forerunner of all physical systems considered for generating quantum light [5, 7–9, 17].

Of particular relevance to this work is the proposal by Lindner and Rudolph [18] for generating one-dimensional photonic cluster states using semiconductor QDs. Their scheme

uses a single QD confined electron spin precessing in a magnetic field while driven by a temporal sequence of picosecond laser pulses. Upon excitation of the QD, a single photon is deterministically emitted, and its polarization is entangled with the state of the QD confined spin. This process repeats many times to generate a large 1D cluster of entangled photons.

Schwartz and coworkers demonstrated a modification of this proposal by generating a 1D cluster state based on QD device and characterizing the cluster entanglement length [19]. The entanglement robustness of such a photonic cluster is mainly determined by the ratio between the optical transition radiative rate and the spin-precession rate [19] and by the coherence properties of the QD spin [20, 21]. The indistinguishability between the emitted photons is mainly determined by the nature of the optical transition, which results in the photon emission [22].

In [19], the entangler was the spin of the QD confined dark exciton (DE) [23]. The short-range electron-hole exchange interaction removes the degeneracy between the two DE spin states. Therefore, a coherent superposition of the DE eigenstates naturally precesses, even without an external magnetic field. Unfortunately, this precession is not easily controlled by external means, limiting the entanglement length. Moreover, the emitted photon leaves the DE in an excited state, having a shorter lifetime than the radiative time. As a result, the emitted photons have limited indistinguishability [22], required for efficient Bell state measurements.

Here we use the heavy-hole (HH) spin [20, 24, 25] as an entangler instead of the DE. The HH has a half-integer spin, and in the absence of a magnetic field, its two spin states are Kramers-degenerate. Therefore its precession rate can be finely controlled by the strength of the external field. As we show below, this allows the optimization of the robustness of the entanglement in the cluster state and determines the photon generation rate. Moreover, in the HH case, the photon leaves the HH in a stable ground state, and therefore, the photons are highly indistinguishable.

We follow Ref. [18], as schematically described in Fig. 1A, by applying a periodic sequence of CNOT- and Hadamard-gates on the HH for producing the cluster state. Fig. 1B and Fig. 1C schematically describe our QD-based device op-

arXiv:2110.05908v1 [quant-ph] 12 Oct 2021

* dg@physics.technion.ac.il

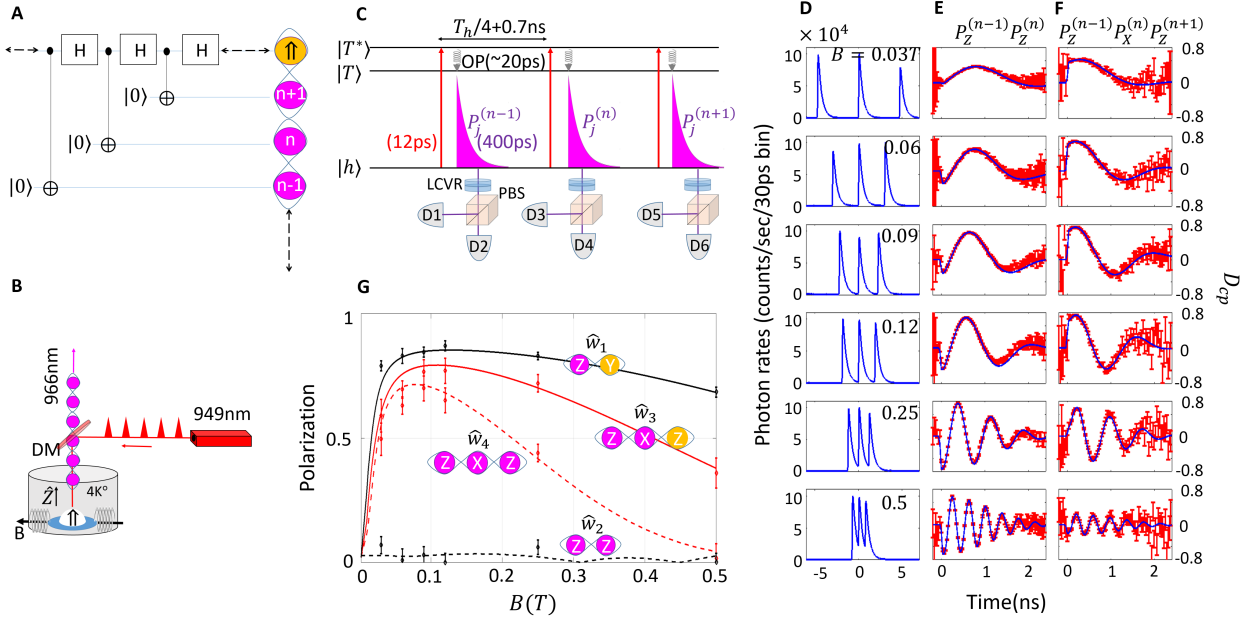


Figure 1: The cluster witnesses. (A) The cluster state is ideally generated by sequential Hadamard-and CNOT-gates. (B) The QD-based device. DM is dichroic-mirror. $\vec{B} = B\hat{x}$ is an external magnetic field. (C) The QD's spin-configurations and transition times during the measurement. $|h\rangle$, $|T\rangle$, and $|T^*\rangle$ are the HH, trion, and excited trion states. Red arrows are laser pulses, curly arrows are optical-phonons, and the pink exponential-decays are the emitted single-photons. T_h is the HH spin-precession period. We detect two and three consequent photons and project their polarization using liquid-crystal-variable-retarders (LCVR) and polarized-beam-splitters (PBS). $P_j^{(i)}$ represents the polarization of the i 's-photon in the cluster, projected on the j polarization state. (D) Time-resolved PL measurements for various magnetic fields. (E) [(F)] 2-photon (3-photon) correlations. Red marks are the time-resolved measurement of the last correlated photon's degree-of-circular-polarization (D_{cp}) as a function of time from the second (third) pulse. Blue lines represent the best fitted central-spin-evolution model for the positive-trion [20, 26]. (G) The measured (error bars) and calculated (color matched lines) cluster-state witnesses as deduced from the fits in (E) and (F) vs. the in-plane magnetic field strength. Strings of polarized photons (pink-) and spin (yellow-) circles describe the witnesses.

eration and the HH-positive trion energy levels. Each laser pulse (red upward arrow) excites the confined HH ($|\uparrow\rangle$) to the excited- positive trion state ($|\uparrow\downarrow\uparrow\rangle^*$), in which the electron resides in its respective second energy level. The electron decays to the trion ground level within about 20 ps by emitting a spin-preserving optical phonon [27]. The trion then recombines within about 400 ps, by emitting a photon (marked in pink), leaving the HH at its ground level. A dichroic mirror steers the emitted photons to the detectors.

Both the HH and the positive trion act as spin qubits [28]. The selection rules for the optical transitions associated with the excitation and emission result in entanglement between the photon polarization and the HH-spin polarization [29]. Therefore each excitation-emission step is an actual realization of a CNOT gate between the spin and the photon qubits. We realize the Hadamard gate on the spin qubit by timing the temporal precession of the HH to match one-quarter of its precession-period plus a small addition compensating for the finite radiative time of the trion. A sequence of resonantly tuned linearly polarized laser π -pulses experimen-

tally realizes the generation of the cluster state (Fig. 1C). Each pulse results in the addition of an entangled photon to the cluster state.

We measure the cluster state's entanglement robustness for various external magnetic fields using three cycles of the cluster protocol and considering events in which three consequent photons are detected. In Fig. 1D, we present these measurements for six different magnetic field strengths. We use the last detected photon for the tomography of the HH-spin. The tomography utilizes time-resolved degree-of-circular-polarization (D_{cp}) measurement for monitoring the trion's spin evolution during its radiative decay back to the HH [26, 30].

Fig. 1E and Fig. 1F show the $D_{cp}(t)$ of the correlated photon-spin states and photon-photon-spin states, respectively, measured for six different magnetic fields. From the fit to these measurements, we extract the following four cluster-state witnesses: $\hat{w}_1 = P_Z^{(n-1)} S_Y$, $\hat{w}_2 = P_Z^{(n-1)} P_Z^{(n)}$, $\hat{w}_3 = P_Z^{(n-1)} P_X^{(n)} S_Z$ and $\hat{w}_4 = P_Z^{(n-1)} P_X^{(n)} P_Z^{(n+1)}$, where $P_j^{(i)}$ represents the polarization projection of the i 's-photon in the

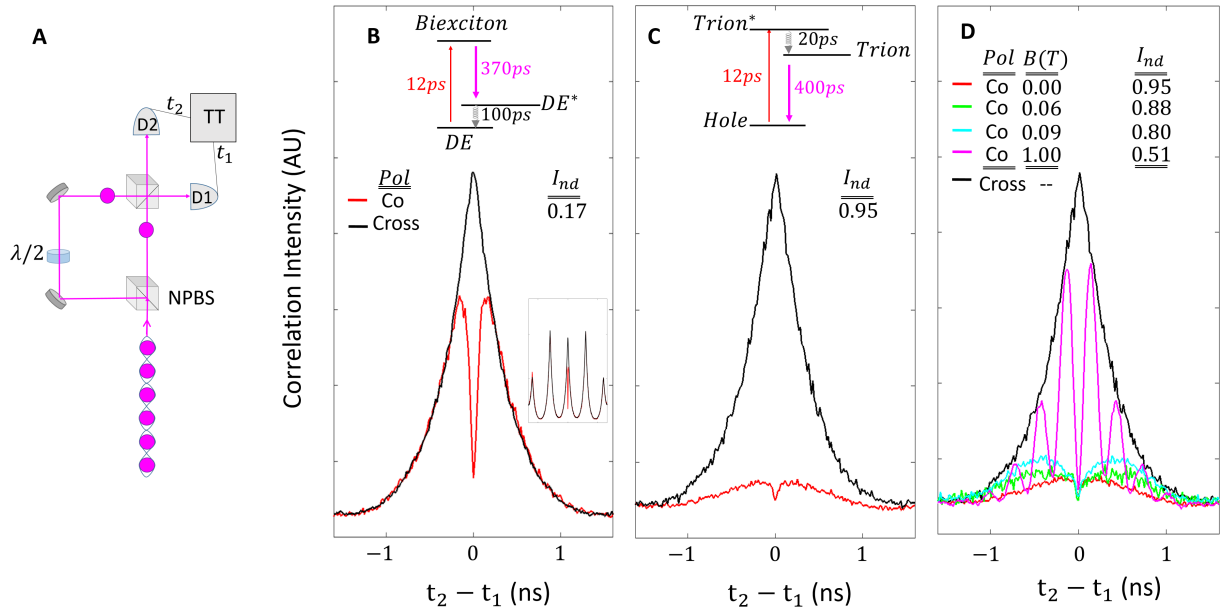


Figure 2: Photon indistinguishability. (A) The interferometer setup. Two consequent cluster-photons interfere on a Non-Polarizing-Beam-Splitter (NPBS). Detectors on the two output ports register the detection times $t_1(t_2)$ of the photons. A half-wave plate ($\lambda/2$) in a rotation mount selects between the two photons' co- or cross-linear polarization state. (B) [(C)] Indistinguishability measurements between two consecutive photons from a cluster where the DE [HH] is the entangler. The solid lines represent the measured second-order correlation function $g^{(2)}(t_2 - t_1)$. The measured indistinguishability is defined as $I_{nd} = 1 - A_{co}/A_{cross}$, where $A_{co}(A_{cross})$ is the area under the co-(cross-) polarized correlation function, represented by the red (black) solid line. The inset in (B) [(C)] describes the energy levels and the transition rates between the levels for the DE [HH]. The bottom inset in (B) describes $g^{(2)}(t_2 - t_1)$ on a 13ns time scale. The interference is visible on the zero-time difference coincidences. (D) Indistinguishability measurements, like in (C) for various externally applied magnetic fields.

string, on the j polarization, and S_j is the polarization of the HH-spin, projected on the j state. We note that \hat{w}_1 and \hat{w}_3 are directly extracted from the polarization of correlated detection of 2- and 3-photons, shown in Fig. 1E and 1F, respectively, while \hat{w}_2 and \hat{w}_4 are extracted from the temporal integration of these measurements. For an ideal cluster-state (containing ideal CNOT and Hadamard gates), \hat{w}_1, \hat{w}_3 , and \hat{w}_4 equal 1, and \hat{w}_2 equals 0.

In Fig. 1G, we present the four measured witnesses as a function of the magnetic field strength. The solid lines are the calculated witnesses using our state-evolution-model [29]. The parameters used for the model calculations were independently measured and listed in Ref. [30]. Very good quantitative agreement between the measured data and the calculations is obtained.

We now turn to measure the indistinguishability between two sequential photons in the cluster state. We use the HOM-setup [31, 32] illustrated in Fig. 2A to compare the indistinguishability resulting from using the DE as entangler (Fig. 2B) with that of the HH (Fig. 2C). The indistinguishability is given by the ratio between the second-order interference of co- to cross-polarized photons. At zero magnetic field, the DE-

cluster photons indistinguishability amounts to 17%, much lower than that of the HH-cluster, which amounts to 95%.

The indistinguishability between photons emitted from a quantum source of single-photons depends on the initial and final states' temporal stability [22]. The insets to Fig. 2B and 2C illustrate the energy level structures and the relevant transition rates for the DE and the HH, respectively. This significant improvement in the indistinguishability of the HH-cluster photons results from the temporal stability of the HH final ground level compared with the excited level of the DE [29].

The externally applied magnetic field reduces the indistinguishability of the HH-cluster photons. Fig. 2D presents indistinguishability measurements of the HH-cluster photons for various magnetic fields. As the field increases, the indistinguishability decreases due to the field-induced spectral broadening. At large fields, when the Zeeman splitting surpasses the radiative linewidth [29], the indistinguishability drops to 50%, and quantum beats are observed in the time-resolved correlation measurements [33].

Fig. 3 summarizes the indistinguishability properties of the cluster photons, the robustness of the generated entanglement,

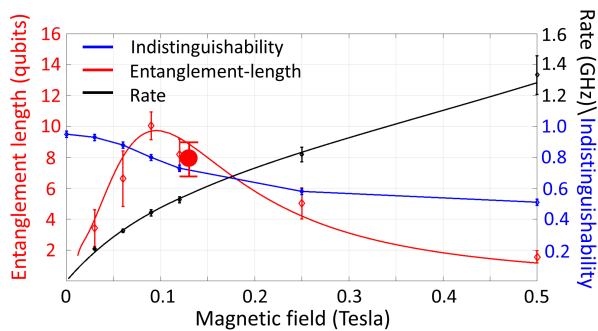


Figure 3: **Cluster characterization.** The cluster state’s localizable-entanglement (LE) characteristic length (red), photon-indistinguishability (blue), and generation rate (black) as a function of the magnetic field. Marked points and error bars are deduced from our measurements. The lines represent calculations in which the process map was obtained from our state-evolution model [29]. The red circle stands for the LE length at $B=0.12\text{T}$, where the process map was measured.

and the photon-generation-rate as a function of the applied magnetic field.

The entanglement robustness is quantified using localizable entanglement (LE) [34], defined as the magnitude of the entanglement between two qubits in the cluster after all the other qubits are projected on suitable bases. The LE decays exponentially with the distance between the two qubits [19, 34]. Thus ζ_{LE} , defined as the characteristic decay-length of the LE, is a figure-of-merit characterizing the robustness of the entanglement in the cluster.

Fig. 3 presents ζ_{LE} vs. the magnetic field strength, where ζ_{LE} is deduced from the ratio between two of the measured witnesses (red diamond marks) according to:

$$\zeta_{LE} = -1/\ln(\hat{w}_3/\hat{w}_1). \quad (1)$$

The difference between these two witnesses is simply the D_{cp} loss due to one application of the process map. For a field strength of 0.12 Tesla, ζ_{LE} (full red circle) was deduced from a full measurement of the process map [29]. The measured ζ_{LE} vs. magnetic field is compared with our central-spin-evolution model (solid red line), using the measured QD-parameters [30].

Fig. 3 clearly shows an optimum for the entanglement robustness at $B_x=0.09$ Tesla, in which $\zeta_{LE} = 10$. For stronger fields, the precession period becomes shorter. As a result, the ratio between the radiative-time and precession-time becomes larger, thereby increasing the deviation of the 2-qubit gate from the ideal CNOT gate. For weaker fields, the precession-time increases. Consequently, the time-difference between

consecutive pulses increases to a level in which the HH-spin dephasing becomes significant.

To complete the device characterization, Fig. 3 presents also the measured indistinguishability (in blue) and the cluster generation rate (in black) vs. the magnetic field strength. The indistinguishability monotonically decreases from 95% as the field increases. This decrease is due to the field-induced broadening of the optical transition. At $B = 0.09$ Tesla, the measured indistinguishability is better than 80%.

The time between consecutive laser pulses is set to approximately match a quarter of a precession period. Therefore, the generation rate monotonically increases as a function of the magnetic field. At the optimal field of 0.09 Tesla, the generation rate is about 0.5 GHz.

The overall detection efficiency of our system is currently better than 1%. The main losses are due to limited light-harvesting efficiency from the planar microcavity containing the QD (~20%), free space into fiber coupling (~50%), detectors quantum efficiency (~80%) and the overall optical-elements transmission efficiency (~10%). With the current system efficiency, we measure four-photon correlations at a few Hertz rate. This detection rate is enough to demonstrate and characterize our cluster-state-generating-device.

There is an obvious need to improve the collection efficiency. A clear way is to integrate the QD into a 3D photonic microcavity [16, 35, 36]. Using such a microcavity with a better mode matching to a single-mode fiber can increase the system efficiency by at least an order of magnitude. In addition, a 3D microcavity can significantly shorten the radiative lifetime due to the Purcell effect. This will significantly improve both the entanglement length and the photon indistinguishability.

In summary, we demonstrate a-Gigahertz rate deterministic-generation of a cluster state of indistinguishable photons using a QD confined HH-spin as an entangler. We show that by optimizing the in-plane external magnetic field, we achieve a characteristic entanglement-length of 10 photons, and photon indistinguishability which is better than 80%. Further feasible optimizations of the device can bring widespread measurement-based implementations of quantum communication and information processing closer.

ACKNOWLEDGMENTS

The support of the Israeli Science Foundation (ISF), and that of the European Research Council (ERC) under the European Union’s Horizon 2020 research and innovation programme (Grant Agreement No. 695188) are gratefully acknowledged.

[1] H.-J. Briegel, W. Dür, J. I. Cirac, and P. Zoller, *Physical Review Letters* **81**, 5932 (1998).

[2] L.-M. Duan, M. D. Lukin, J. I. Cirac, and P. Zoller, *Nature* **414**, 413 (2001).

- [3] S. Wehner, D. Elkouss, and R. Hanson, *Science* **362**, 303 (2018).
- [4] R. Raussendorf and H. J. Briegel, *Physical Review Letters* **86**, 5188 (2001).
- [5] M. Zwerger, W. Dür, and H. J. Briegel, *Physical Review A* **85**, 062326 (2012).
- [6] M. Hein, J. Eisert, and H. J. Briegel, *Physical Review A* **69**, 062311 (2004).
- [7] D. Buterakos, E. Barnes, and S. E. Economou, *Physical Review X* **7**, 041023 (2017).
- [8] K. Azuma, K. Tamaki, and H.-K. Lo, *Nature Communications* **6**, 6787 (2015).
- [9] W. J. Munro, A. M. Stephens, S. J. Devitt, K. A. Harrison, and K. Nemoto, *Nature Photonics* **6**, 777 (2012).
- [10] M. V. Larsen, X. Guo, C. R. Breum, J. S. Neergaard-Nielsen, and U. L. Andersen, *Science* **366**, 369 (2019).
- [11] J.-P. Li, J. Qin, A. Chen, Z.-C. Duan, Y. Yu, Y. Huo, S. Höfling, C.-Y. Lu, K. Chen, and J.-W. Pan, *ACS Photonics* **7**, 1603 (2020).
- [12] D. Istrati, Y. Pilnyak, J. C. Loredó, C. Antón, N. Somaschi, P. Hilaire, H. Ollivier, M. Esmann, L. Cohen, L. Vidro, C. Millet, A. Lemaître, I. Sagnes, A. Harouri, L. Lanco, P. Senellart, and H. S. Eisenberg, *Nature Communications* **11**, 5501 (2020).
- [13] J.-C. Besse, K. Reuer, M. C. Collodo, A. Wulff, L. Wernli, A. Copetudo, D. Malz, P. Magnard, A. Akin, M. Gabureac, G. J. Norris, J. I. Cirac, A. Wallraff, and C. Eichler, *Nature Communications* **11**, 4877 (2020).
- [14] A. Aspect, P. Grangier, and G. Roger, *Physical Review Letters* **49**, 91 (1982).
- [15] N. Akopian, N. H. Lindner, E. Poem, Y. Berlatzky, J. Avron, D. Gershoni, B. D. Gerardot, and P. M. Petroff, *Physical Review Letters* **96**, 130501 (2006).
- [16] P. Senellart, G. Solomon, and A. White, *Nature Nanotechnology* **12**, 1026 (2017).
- [17] M. H. Appel, A. Tiranov, A. Javadi, M. C. Löbl, Y. Wang, S. Scholz, A. D. Wieck, A. Ludwig, R. J. Warburton, and P. Lodahl, *Physical Review Letters* **126**, 013602 (2021).
- [18] N. H. Lindner and T. Rudolph, *Physical Review Letters* **103**, 113602 (2009).
- [19] I. Schwartz, D. Cogan, E. R. Schmidgall, Y. Don, L. Gantz, O. Kenneth, N. H. Lindner, and D. Gershoni, *Science* **354**, 434 (2016).
- [20] D. Cogan, O. Kenneth, N. H. Lindner, G. Peniakov, C. Hopfmann, D. Dalacu, P. J. Poole, P. Hawrylak, and D. Gershoni, *Physical Review X* **8**, 041050 (2018).
- [21] A. Bechtold, D. Rauch, F. Li, T. Simmet, P.-L. Ardelit, A. Regler, K. Müller, N. A. Sinitsyn, and J. J. Finley, *Nature Physics* **11**, 1005 (2015).
- [22] A. Kiraz, M. Atatüre, and A. Imamoglu, *Physical Review A* **69**, 032305 (2004).
- [23] I. Schwartz, E. R. Schmidgall, L. Gantz, D. Cogan, E. Bordo, Y. Don, M. Zielinski, and D. Gershoni, *Physical Review X* **5**, 011009 (2015).
- [24] B. D. Gerardot, D. Brunner, P. A. Dalgarno, P. Öhberg, S. Seidl, M. Kroner, K. Karrai, N. G. Stoltz, P. M. Petroff, and R. J. Warburton, *Nature* **451**, 441 (2008).
- [25] D. Brunner, B. D. Gerardot, P. A. Dalgarno, G. Wüst, K. Karrai, N. G. Stoltz, P. M. Petroff, and R. J. Warburton, *Science* **325**, 70 (2009).
- [26] D. Cogan, G. Peniakov, Z.-E. Su, and D. Gershoni, *Physical Review B* **101**, 035424 (2020).
- [27] Y. Benny, Y. Kodriano, E. Poem, D. Gershoni, T. A. Truong, and P. M. Petroff, *Physical Review B* **86**, 085306 (2012).
- [28] D. Loss and D. P. DiVincenzo, *Physical Review A* **57**, 120 (1998).
- [29] “See supplementary materials;”.
- [30] D. Cogan, Z.-E. Su, O. Kenneth, and D. Gershoni, arXiv:2108.05173 (2021), <http://arxiv.org/abs/2108.05173v1>.
- [31] C. K. Hong, Z. Y. Ou, and L. Mandel, *Physical Review Letters* **59**, 2044 (1987).
- [32] C. Santori, D. Fattal, J. Vučković, G. S. Solomon, and Y. Yamamoto, *Nature* **419**, 594 (2002).
- [33] T. Legero, T. Wilk, M. Hennrich, G. Rempe, and A. Kuhn, *Physical Review Letters* **93**, 070503 (2004).
- [34] F. Verstraete, M. Popp, and J. I. Cirac, *Physical Review Letters* **92**, 027901 (2004).
- [35] F. Liu, A. J. Brash, J. O’Hara, L. M. P. P. Martins, C. L. Phillips, R. J. Coles, B. Royall, E. Clarke, C. Bentham, N. Prtljaga, I. E. Itskevich, L. R. Wilson, M. S. Skolnick, and A. M. Fox, *Nature Nanotechnology* **13**, 835 (2018).
- [36] N. Tomm, A. Javadi, N. O. Antoniadis, D. Najer, M. C. Löbl, A. R. Korsch, R. Schott, S. R. Valentin, A. D. Wieck, A. Ludwig, and R. J. Warburton, *Nature Nanotechnology* **16**, 399 (2021).

Supplemental material for "A deterministic source of indistinguishable photons in a cluster state"

Dan Cogan, Zu-En Su, Oded Kenneth, and David Gershoni*

The Physics Department and the Solid State Institute,

Technion–Israel Institute of Technology, 3200003 Haifa, Israel

* dg@physics.technion.ac.il

CONTENTS

SM1. The sample and optical system	2
SM2. The state-evolution model	3
SM3. Measuring the process map of the repeated cycle of the protocol	6
SM4. Estimation of the photon indistinguishability.	9
SM5. The X^{+1} optical transitions in the presence of an externally applied in-plane magnetic field.	9
References	11

SM1. THE SAMPLE AND OPTICAL SYSTEM

In the heart of our device is an InGaAs self assembled semiconductor quantum dot (QD), as illustrated in Fig. 1B in the main article. The QD contains a confined heavy-hole (HH) spin qubit [1–5]. We define the QD’s shortest dimension ($\sim 3\text{nm}$), the growth direction, and the spin quantization axis as the Z-axis. The externally applied magnetic field direction is defined as the X-axis. The QD is embedded in a planar microcavity, formed by 2 Bragg-reflecting mirrors, facilitating light-harvesting efficiency of about 20% by a 0.85 numerical aperture objective above the QD.

The experimental system is described in Ref. [5]. A modified version is schematically described in Fig. S1. The pulsed laser light is resonantly tuned to the HH-excited trion optical transition [6], and its power is set to a π -area intensity. The polarization of the light is computer-controlled using pairs of liquid crystal variable retarders (LCVRs) and polarizing beam splitters (PBS). Very weak above bandgap CW light is also used to stabilize the charge state of the QD [5]. Similar sets of LCVRs and PBSs are used to project the polarization of the collected photons on 6 different polarization bases. We use highly efficient transmission

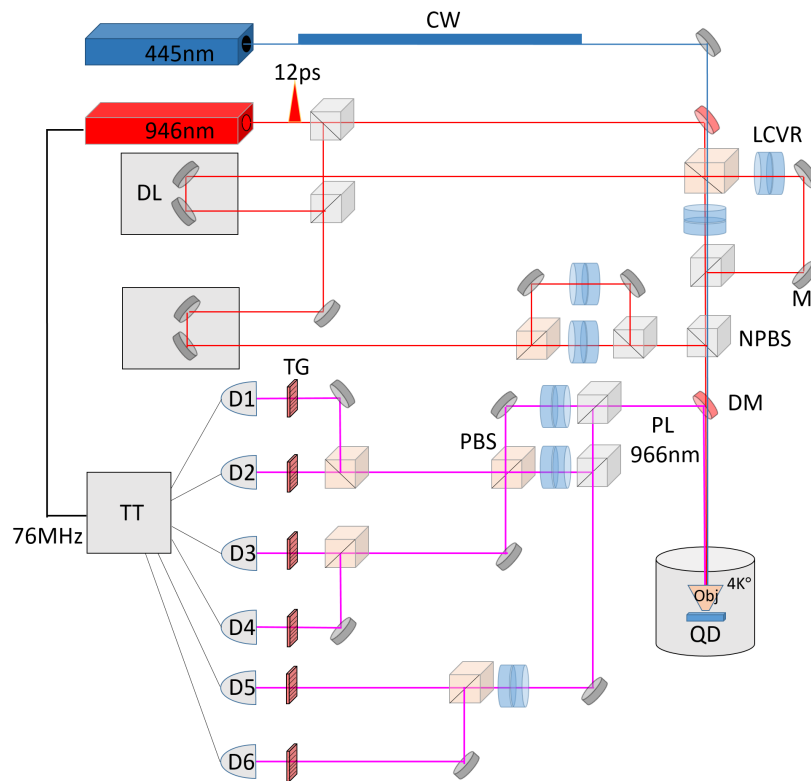


Figure S1: **The experimental system.** CW, continuous wave; DL, Delay line; M, mirror; DM, dichroic mirror; NPBS, non-polarizing beam splitter; PBS, polarizing beam splitter; OBJ, microscope objective; LCVR, liquid crystal variable retarder; D_n, single-photon detector n; TT, Time tagging correlation module;

gratings to spectrally filter the emitted photons. The filtered photons are detected using efficient (>80%) single-photon superconducting detectors, with temporal resolution of about 30ps. The photons detection times are recorded using time tagging correlation module.

SM2. THE STATE-EVOLUTION MODEL

Here we outline the state evolution model, which describes the actual single cycle of the periodic protocol. The cycle is ideally composed of two gates. A CNOT gate between the QD spin-qubit and the emitted photon polarization-qubit, followed by a Hadamard gate acting

on the spin qubit only. The CNOT gate is realized by the pulsed optical excitation of the HH spin and the resulting single-photon emission. The Hadamard gate is realized by the timed free coherent precession of the HH around the direction of the externally applied magnetic field. We developed the state evolution model in order to realistically describe the process map and its deviation from the ideal map, composed of the ideal gates.

The optical excitation of the HH results in a positively charged trion composed of two paired holes and a single electron (Fig. S2A). The two holes and the single electron spins interact via the hyperfine interaction with nuclear spins in their vicinity and with the externally applied magnetic field. In Ref. [6], we developed a model that quantitatively describes both spins' evolution under these conditions, focusing particularly on the relevant regime, where the external field is comparable in magnitude to one standard deviation of the effective nuclear magnetic field (Overhauser field) due to random statistical fluctuations in the nuclei spins [7].

In Ref. [6], we show that under these conditions the central spin $\vec{S}(t)$ evolution is given by:

$$\vec{S}(t) = \bar{G}\vec{S}_0 \quad (1)$$

where $\vec{S}_0 = \vec{S}(0)$ is the central spin initial value and \bar{G} is a 3×3 tensor whose elements can be calculated numerically as explained in Ref [6]. We mark by \bar{G}^{HH} and \bar{G}^{trion} the tensors for the HH and trion.

Each cycle starts with an initial HH spin state \vec{S}_0 , which is the state in which the HH was left at the end of the previous cycle. The photons emitted by the QD during previous cycles can be safely disregarded.

A 12ps π -area laser pulse converts the HH state to an excited positive trion state. The optical transitions between these two spin qubits are governed by the following Π -system optical polarization selection rules [5]:

$$\begin{aligned} |\uparrow\rangle &\xleftrightarrow{|-Z\rangle} |\uparrow\downarrow\uparrow\rangle, \\ |\downarrow\rangle &\xleftrightarrow{|+Z\rangle} |\downarrow\uparrow\downarrow\rangle. \end{aligned} \quad (2)$$

where $|+Z\rangle$ and $|-Z\rangle$ are photons with right and left circular polarizations or angular momentum of +1 and -1, respectively along the z-direction. Since our short laser pulses can be considered instantaneous it follows that a short laser pulse polarized $|+X\rangle = (|+Z\rangle + |-Z\rangle) / \sqrt{2}$, coherently converts the HH spin state into a similar trion state[6, 8]. described by \vec{S}_0 . The trion then radiatively decays exponentially ($\sim e^{-t/\tau_{photon}}$ with $\tau_{photon} = 400$ ps) into an entangled HH+photon state.

We proceed by separating the temporal evolution into three domains: the trion evolution before the emission, the emission itself and the HH evolution after the emission. The evolution during the first and third domains is described by Eq. 1. In the following we discuss the second part which includes both qubits: the emitted photon and the spin.

Note that while above we used \vec{S} to describe the QD spin, an equivalent description in terms of a density matrix is

$$\hat{\rho}_{2 \times 2} = \frac{1}{2} (\hat{\sigma}_0 + S_x \hat{\sigma}_x + S_y \hat{\sigma}_y + S_z \hat{\sigma}_z) \quad (3)$$

with $\hat{\sigma}_i$ being the Pauli matrices and $\hat{\sigma}_0$ the identity matrix. According to the polarization selection rules for the optical transition between the trion and the HH spins, described by Eq. 2, a photon emission occurring right after the moment $t = t'_+$, results in the spin+photon state

$$\hat{\rho}_{4 \times 4}(t'_+) = \begin{bmatrix} 0 & & \\ & \hat{\rho}_{2 \times 2}(t'_-) & \\ & & 0 \end{bmatrix}. \quad (4)$$

Projecting this on the photon state $\frac{1}{2}(I + \vec{m} \cdot \vec{\sigma})$, where \vec{m} is the photon's normalized Stokes vector, we obtain after tracing over the photon, the HH state

$$\frac{1}{2} \begin{bmatrix} (1 + S_z)(1 - m_3) & (S_x - iS_y)(m_1 - im_2) \\ (S_x + iS_y)(m_1 + im_2) & (1 - S_z)(1 + m_3) \end{bmatrix}. \quad (5)$$

where $\vec{S} = \vec{S}^{trion}(t'_-)$ right before the photon emission. The (trace) normalization of this gives the probability $p = \frac{1}{2}(1 - S_z m_3)$ to find the photon \hat{m} -polarized and the expectation value of $\vec{\sigma}$ gives the HH spin

$$p \vec{S}^{HH}(t'_+) = \frac{1}{2} (m_1 S_x - m_2 S_y, m_1 S_y + m_2 S_x, S_z - m_3) \quad (6)$$

We may write this as $p\vec{S}^{HH}(t'_+) \equiv \bar{T}^m \vec{S}^{trion}(t'_-)$ where \bar{T}^m is defined by Eq. 6. Note that \bar{T}^m is an affine rather than a linear transformation.

Collecting everything together, this suggests that the spin at the end of the cycle (occurring at the moment t_{pulse} of the next pulse) should satisfy

$$P^{(m)} \langle \vec{S}(t_{pulse}) \rangle = \frac{1}{\tau_{photon}} (1 - e^{-\frac{t_{pulse}}{\tau_{photon}}}) \quad (7)$$

$$\int d\mathcal{P} \int_0^{t_{pulse}} e^{-\frac{t'}{\tau_{photon}}} dt' \bar{G}^{HH}(t_{pulse} - t') \bar{T}^m \bar{G}^{trion}(t') \vec{S}_0 b$$

where

$$d\mathcal{P} = \frac{1}{(2\pi)^{3/2}} \exp\left(-\frac{1}{2}B^2\right) d^3B \quad (8)$$

is the probability element of the normalized nuclear field [6], and $P^{(m)}$ is the probability to find the emitted photon \hat{n} -polarized. $P^{(m)}$ may be obtained from

$$1 - 2P^{(m)} = \frac{m_3}{\tau_{photon}} (1 - e^{-\frac{t_{pulse}}{\tau_{photon}}}) \quad (9)$$

$$\int d\mathcal{P} \int_0^{t_{pulse}} e^{-\frac{t'}{\tau_{photon}}} dt' \left(\hat{z} \cdot \bar{G}^{trion}(t') \vec{S}_0 \right).$$

In practice $e^{-\frac{t_{pulse}}{\tau_{photon}}} \ll 1$ may be safely neglected.

We solve the integrals in Eq. 7,9 numerically[9] with the QD carriers' g-factor and hyperfine tensors as measured independently and described elsewhere [6].

We use this model to calculate the expected values of the four cluster-state witnesses displayed in Fig. 1G of the main article. Similarly, we use the model for calculating the expected process map [10] and the localizable entanglement characteristic length [11, 12] as a function of the externally applied magnetic field, as displayed in Fig. 3 of the main article. As can be seen in both figures the model quite accurately describes the measurements.

SM3. MEASURING THE PROCESS MAP OF THE REPEATED CYCLE OF THE PROTOCOL

As discussed above, the cluster state is generated by repeatedly applying the same process on the QD confined spin. This means that one can fully characterize the cluster quantum state

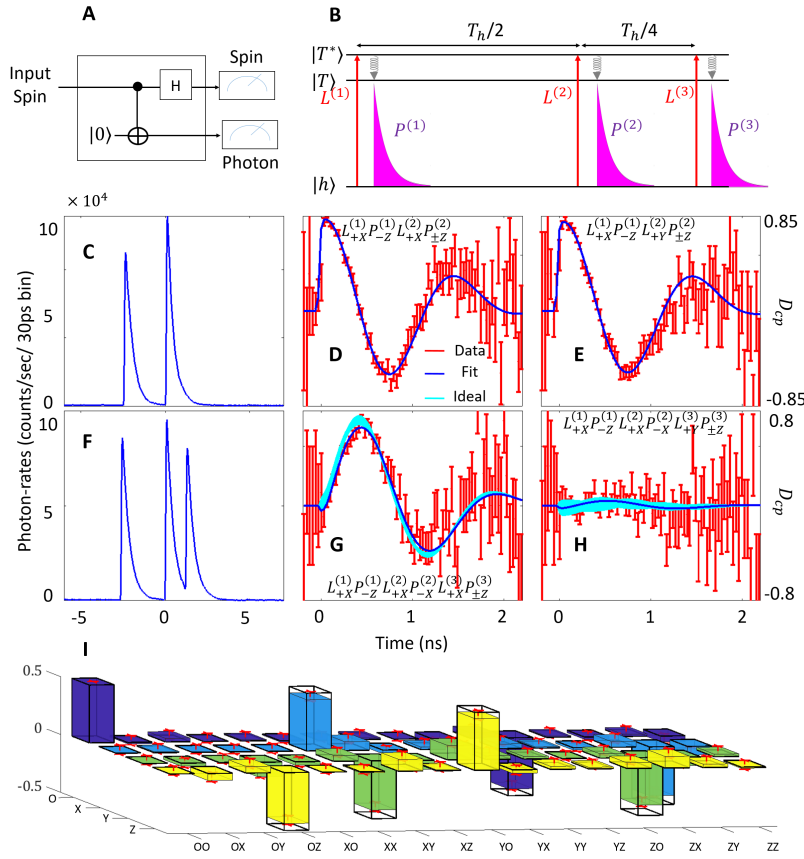


Figure S2: Measurement of the process map for an applied magnetic field of 0.12T. (A) Schematics description of the process map acting on the HH spin. (B) Schematic description of the pulse sequence and resulted photon emission used for measuring the process map elements for initialized HH spin $|\pm Z\rangle$ states. $L_i^{(n)}$ ($P_i^{(n)}$) mark the n's laser pulse (single-photon detected) where i marks the polarization. (C, D-E) Time resolved emission and degree-of-circular-polarizations (D_{cp}) measurements for characterizing the HH $|+Z\rangle$ input spin state. (F, G-H) Time resolved emission and D_{cp} measurements for characterizing the spin+photon state, resulting from application of the process map on the $|+Z\rangle$ input spin state. The red error-bars constitute one standard deviation of the experimental uncertainty. The blue lines represent the best fitted model results [8]. The light-blue lines represent the expected results assuming ideal process map. (I) The measured (filled colored bars) and ideal (empty bars) process map. X, Y, Z, and O stands for the corresponding Pauli and identity matrices basis representation, respectively.

for any number of qubits if the process-map is accurately known [10, 12]. The process map, which is schematically described in Fig. S2A, maps the spin qubit state into an entangled spin-photon two qubit state. Since the spin quantum state can be fully described by a 2x2 density matrix and the spin+photon state by a 4x4 density matrix, it follows that the process map can be fully described by a 4x16 positive and trace-preserving matrix which contains 64 real matrix elements, as presented in Fig. S2A.

In Ref. [10] we describe a novel way for obtaining the process map from a set of time resolved polarization sensitive two and three photon correlation measurements. In Fig. S2B, we schematically describe the experimental method where we used a 2-pulse-experiment to initialize and HH spin qubit and then to measure the resulting HH quantum state [8]. Similarly, a 3-pulse-experiment is used to initialize the HH spin, apply one cycle of the process on the initialized spin and then to measure the resulted entangled spin+photon state.

In Fig. S2C we present time-resolved two-pulse-correlation-measurements in which the input HH was initialized to $|+Z\rangle$ state and then its state was measured [8]. Fig. S2D and E show the measured time resolved degree of circular polarization ($D_{cp}(t)$) of the emission resulting from a second pulse polarized +X and +Y respectively.

Similarly, we initialize the HH-state to six different states from three orthogonal bases [10, 13]. For each of those 6 states, we used 2 $D_{cp}(t)$ two-photon correlation measurements (not shown) like the measurements displayed in Fig. S2D and E for tomography.

Fig. S2F shows time-resolved three-pulse-correlation-measurement where one cycle of the process is applied to the $|+Z\rangle$ input state and the resulting spin+photon state is measured. In this experiment, the second photon is projected on the -X polarization. Fig. S2G and H show the time resolved $D_{cp}(t)$ of the three-photon correlations measurements resulting from a third pulse polarized +X and +Y, respectively [8].

Fig. S2I shows the results of the full-tomographic measurements of the process map. For acquiring these measurements, for the 6 HH spin initializations, we applied one cycle of the protocol and measured the resulting spin+photon state by projecting both the spin and the photon on different orthogonal polarization bases [14]. For characterizing each of these 6

spin+photon states, we used 12 $D_{cp}(t)$ 3-photon correlations measurements like the ones presented in Fig. S2G and H.

Lastly, in order to obtain the physical process map that best fits our measured results, we use a novel minimization method [10]. In Fig. S2I we compare between the obtained process-map and the ideal one. The fidelity [12, 15] of the measured map to the ideal one is 0.9.

SM4. ESTIMATION OF THE PHOTON INDISTINGUISHABILITY.

The indistinguishability between photons emitted from a quantum source of single-photons depends on the initial and final states’ temporal stability. The indistinguishability, can be roughly estimated by [16, 17]:

$$I_{nd} = [(1 + \tau_{photon}/\tau_{final})(1 + \tau_{init}/\tau_{photon})]^{-1} \quad (10)$$

In Eq. 10, τ_{init} is the initial state’s generation-time (“jitter”), τ_{final} is the final state’s lifetime, and τ_{photon} is the photon’s radiative lifetime. To achieve high indistinguishability, $\tau_{init}/\tau_{photon}$ should be minimized while $\tau_{final}/\tau_{photon}$ should be maximized.

The insets to Fig. 2B and 2C in the main article illustrate the energy level structures and the relevant transition times for the DE and for the HH, respectively. Using these rates in Eq. 10 results in indistinguishability of about 20% for the DE-cluster and 95% for the HH-Trion photons. These estimates agree with the experimental results of 17% and 95% for the DE and HH, respectively, presented in the main article.

SM5. THE X^{+1} OPTICAL TRANSITIONS IN THE PRESENCE OF AN EXTERNALLY APPLIED IN-PLANE MAGNETIC FIELD.

The externally applied magnetic field reduces the indistinguishability of the HH-cluster photons. In Fig. S3A, we schematically describe the HH and positive-trion energy levels and the selection rules for optical transitions between these levels in the presence of an in-plane magnetic field. The field lifts the degeneracy of both the HH and the trion qubits. The resulted HH

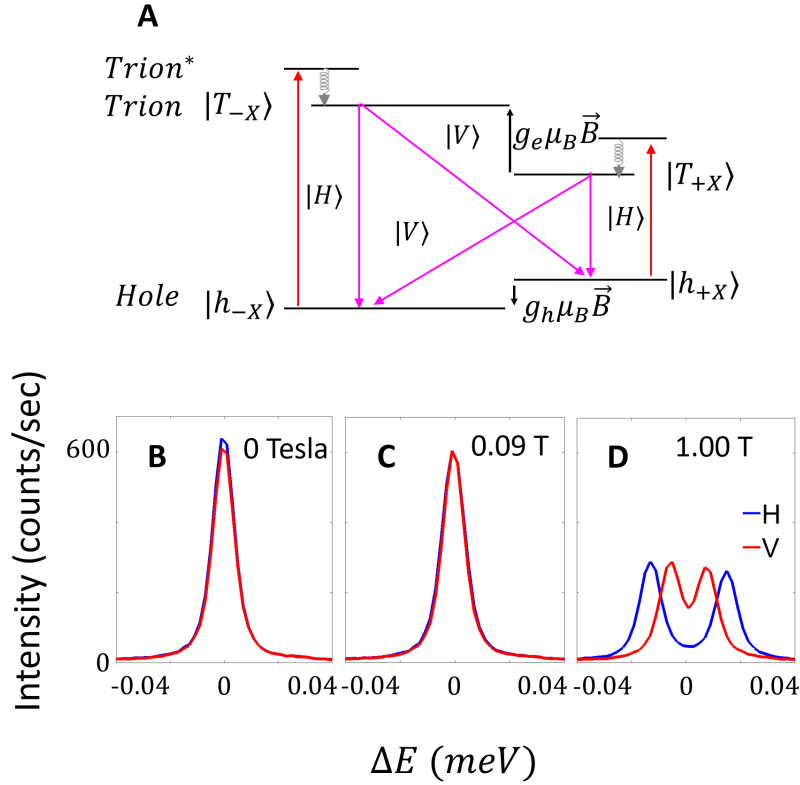


Figure S3: **Spectroscopy of the positive trion (X^{+1}) in the presence of externally applied in-plane magnetic field.** (A) Schematics of the Trion-HH energy levels and optical transitions in the presence of an in-plane external magnetic field. Here $H=X$ ($V=Y$) describes horizontally (vertically) rectilinearly polarized optical transition. (B-D) Polarization-sensitive PL spectral measurements of the Trion-HH transition for various magnetic-fields.

precession is used for implementing the Hadamard gate on the spin. The precession of the trion is used for tomography of the spin qubit [8]. In Fig. S3B-D, we show polarization-sensitive spectral measurements of the X^{+1} spectral line for various magnetic fields. Without a magnetic field, the line is completely degenerate. For a small field of 0.09 Tesla, the degeneracy removal results in a small broadening of the spectral line. This degeneracy removal is more than enough, however, for our purpose, as shown in the main text. For a field of 1.00 Tesla, the spectral line is split into four components, rectilinearly cross-polarized, in perfect agreement with the scheme

of Fig. S3A.

Fig. 2D in the main article presents indistinguishability measurements of the HH-cluster photons for various magnetic fields. As the field increases, the indistinguishability decreases due to the field-induced spectral broadening. At large fields, when the Zeeman splitting surpasses the radiative linewidth, quantum beats are observed in the time-dependent correlation measurements [18]. The quantum beats oscillation frequency exactly matches the energy difference between the V-polarized components of the X^{+1} line in Fig. S3D.

-
- [1] D. Loss and D. P. DiVincenzo, *Physical Review A* **57**, 120 (1998).
- [2] D. P. DiVincenzo, *Fortschritte der Physik* **48**, 771 (2000).
- [3] B. D. Gerardot, D. Brunner, P. A. Dalgarno, P. Öhberg, S. Seidl, M. Kroner, K. Karrai, N. G. Stoltz, P. M. Petroff, and R. J. Warburton, *Nature* **451**, 441 (2008).
- [4] D. Brunner, B. D. Gerardot, P. A. Dalgarno, G. Wüst, K. Karrai, N. G. Stoltz, P. M. Petroff, and R. J. Warburton, *Science* **325**, 70 (2009).
- [5] D. Cogan, O. Kenneth, N. H. Lindner, G. Peniakov, C. Hopfmann, D. Dalacu, P. J. Poole, P. Hawrylak, and D. Gershoni, *Physical Review X* **8**, 041050 (2018).
- [6] D. Cogan, Z.-E. Su, O. Kenneth, and D. Gershoni, arXiv:2108.05173 (2021), <http://arxiv.org/abs/2108.05173v1>.
- [7] I. A. Merkulov, A. L. Efros, and M. Rosen, *Physical Review B* **65**, 205309 (2002).
- [8] D. Cogan, G. Peniakov, Z.-E. Su, and D. Gershoni, *Physical Review B* **101**, 035424 (2020).
- [9] For certain specific photon polarizations \hat{m} , one may show analytically that some components of the integral vanish by reflection symmetries.
- [10] D. Cogan, G. Peniakov, O. Kenneth, Y. Don, and D. Gershoni, arXiv:2108.05919 (2021), <http://arxiv.org/abs/2108.05919v1>.
- [11] F. Verstraete, M. Popp, and J. I. Cirac, *Physical Review Letters* **92**, 027901 (2004).
- [12] I. Schwartz, D. Cogan, E. R. Schmidgall, Y. Don, L. Gantz, O. Kenneth, N. H. Lindner, and D. Gershoni, *Science* **354**, 434 (2016).

- [13] I. Schwartz, D. Cogan, E. R. Schmidgall, L. Gantz, Y. Don, M. Zieliński, and D. Gershoni, *Physical Review B* **92**, 201201 (2015).
- [14] D. F. V. James, P. G. Kwiat, W. J. Munro, and A. G. White, *Physical Review A* **64**, 052312 (2001).
- [15] R. Jozsa, *Journal of Modern Optics* **41**, 2315 (1994).
- [16] A. Kiraz, M. Atatüre, and A. Imamoğlu, *Physical Review A* **69**, 032305 (2004).
- [17] L. Gantz, D. Cogan, I. Schwartz, E. Schmidgall, G. Bahir, and D. Gershoni, in *Conference on Lasers and Electro-Optics* (OSA, 2017).
- [18] T. Legero, T. Wilk, M. Hennrich, G. Rempe, and A. Kuhn, *Physical Review Letters* **93**, 070503 (2004).